Catalysts **2015**, *5*, 815-837; doi:10.3390/catal5020815

OPEN ACCESS

catalysts

ISSN 2073-4344

www.mdpi.com/journal/catalysts

Article

Electrochemical Oxidation of the Carbon Support to Synthesize Pt(Cu) and Pt-Ru(Cu) Core-Shell Electrocatalysts for Low-Temperature Fuel Cells

Griselda Caballero-Manrique, Enric Brillas, Francesc Centellas, José Antonio Garrido, Rosa María Rodríguez and Pere-Lluís Cabot *

Laboratori d'Electroquímica dels Materials i del Medi Ambient, Departament de Química Física, Universitat de Barcelona, Martí i Franquès 1-11, 08028 Barcelona, Spain;
E-Mails: g_caballe@hotmail.com (G.C.-M.); brillas@ub.edu (E.B.); facentellas@ub.edu (F.C.); joseagarrido@ub.edu (J.A.G.); rosarodriguez@ub.edu (R.M.R.)

* Author to whom correspondence should be addressed; E-Mail: p.cabot@ub.edu; Tel.: +34-93-403-92-36; Fax: +34-93-402-12-31.

Academic Editor: Minhua Shao

Received: 19 January 2015 / Accepted: 22 April 2015 / Published: 30 April 2015

Abstract: The synthesis of core-shell Pt(Cu) and Pt-Ru(Cu) electrocatalysts allows for a reduction in the amount of precious metal and, as was previously shown, a better CO oxidation performance can be achieved when compared to the nanoparticulated Pt and Pt-Ru ones. In this paper, the carbon black used as the support was previously submitted to electrochemical oxidation and characterized by XPS. The new catalysts thus prepared were characterized by HRTEM, FFT, EDX, and electrochemical techniques. Cu nanoparticles were generated by electrodeposition and were further transformed into Pt(Cu) and Pt-Ru(Cu) core-shell nanoparticles by successive galvanic exchange with Pt and spontaneous deposition of Ru species, the smallest ones being 3.3 nm in mean size. The onset potential for CO oxidation was as good as that obtained for the untreated carbon, with CO stripping peak potentials about 0.1 and 0.2 V more negative than those corresponding to Pt/C and Ru-decorated Pt/C, respectively. Carbon oxidation yielded an additional improvement in the catalyst performance, because the ECSA values for hydrogen adsorption/desorption were much higher than those obtained for the non-oxidized carbon. This suggested a higher accessibility of the Pt sites in spite of having the same nanoparticle structure and mean size.

Keywords: electrochemical oxidation of carbon; core-shell Pt(Cu) nanoparticles; core-shell Pt-Ru(Cu)nanoparticles; Pt deposition by galvanic exchange; Ru spontaneous deposition; hydrogen adsorption/desorption; CO oxidation; XPS; HRTEM

1. Introduction

The Proton Exchange Membrane Fuel Cells (PEMFCs) are considered good environmentally friendly alternatives to the use of fossil fuel engines as power generation systems for transport applications. They have better energy efficiency, lower operation temperature, and much lower emission of pollutants [1–4]. One of the problems appears when using hydrogen obtained from reforming, because it contains CO, which is strongly adsorbed on Pt. This produces the metal poisoning and decreases the anode performance. On the other hand, Direct Methanol Fuel Cells (DMFCs) are envisaged for low-weight portable applications such as laptops, cellular phones, sensors, and medical devices, in which the methanol fuel can be easily managed and recharged [4–8]. In this case, the anodic oxidation of methanol produces CO-type intermediates, which also lead to the Pt metal poisoning. In order to solve this problem, Pt-containing binary and ternary alloys have alternatively been studied [3,5,9–15]. The amount of Pt used could also be decreased in this form, because it is expensive and has a limited abundance in the Earth [3,7,8,11,16–18]. In this way, Pt-Ru and Pt alloy nanoparticles containing Au, Ni, Cu, Co, Pd, and/or other transition metals have been tested on different carbon substrates as anodic catalysts [1,2,6,9–11,13,16,17,19–29].

Many different allotropic forms of carbon have been used as substrates to synthesize Pt-based catalysts. Pt(IV) and Ru(III) species or their carbonyl complexes can be reduced in ethylenglycol or formate solutions [11,13,30], also using in some cases oil in water microemulsions [31], microwave radiation [15], or galvanic exchange [32–34]. However, carbon blacks and active carbons have been the mostly employed supports for low-temperature fuel cells due to their unique characteristics of high surface area, electric conductivity, porosity, stability, and low cost [1,3,10,16,22,30,35,36]. The morphology and size distribution of carbon black particles depend on the raw material and on the thermal decomposition process utilized in the synthesis procedure. Vulcan carbons XC-72 and XC-72R [37] are carbon blacks obtained from the pyrolysis of natural gas or oil fractions. They can be considered rather graphitic amorphous forms of carbon with spherical shape about 50 nm in diameter that can be aggregated in spherules of about 250 nm in size [30,36]. Vulcan XC-72R has suitable surface and micropore areas of 218 and 65.2 m^2g^{-1}, respectively, and pore, mesopore, and micropore volumes of 0.41, 0.3,7 and 0.036 cm^3g^{-1}, respectively [19,37,38].

It has been noted that carbon blacks have a large number of diverse structural defects that affect their reproducibility as substrates [1,8,19,39]. For this reason, these carbons are normally functionalized by means of surface oxidation treatments to create oxygenated organic groups that can serve as nucleation points for the metallic precursors. The oxygenated groups help to diminish the carbon hydrophobicity, thereby favoring the accessibility of the aqueous metallic precursors. On the other hand, the less acidic groups increase the interaction between the metal precursor and the carbon support, thus avoiding the agglomeration tendency of the metal on the carbon [1,40]. The functionalization of the carbon surface

can be achieved by treatment with strong oxidizing acids such as nitric, sulfuric, phosphoric, sulphonic, or their mixtures, or by means of sodium hydroxide, ammonia, or hydrogen peroxide [18,27–29,35,36,38,40–46]. Oxygen or oxygen plus nitrogen mixtures, thermal oxidation [18,38], and electrochemical oxidation at constant current or potential, potential pulses, or potential cycling have also been applied [28,34,42,45,47]. All these techniques were able to introduce oxygenated surface compounds via the consecutive formation of hydroxyl, carbonyl, and carboxyl groups according to the following reaction sequence [47]:

$$=\overset{\downarrow}{C}\text{-H}\rightarrow=\overset{\downarrow}{C}\text{-OH}\rightarrow>\text{C=O}\rightarrow\text{–COOH} \quad (1)$$

Hydroquinone (HQ) $C_6H_4(OH)_2$ groups, which can be oxidized to quinone (Q) $C_6H_4O_2$ groups, can also improve the electrocatalytic properties and the stability of the catalysts in the operation conditions of the fuel cells [18,19,35,36,38,42–45]:

$$HQ \rightarrow Q + 2H^+ + 2e^- \quad (2)$$

However, extreme oxidizing conditions under high temperature, humidity, and low pHs can negatively affect the performance and durability of the PEM anodes because carbon can be oxidized to CO and CO_2 according to the following reactions [19]:

$$C(s) + H_2O \rightarrow CO_{(g)} + 2H^+ + 2e^- \quad (3)$$

$$C(s) + 2H_2O \rightarrow CO_{2(g)} + 4\,H^+ + 4e^- \quad (4)$$

To the best of the authors' knowledge, studies about the effect of carbon oxidation as a substrate for copper electrodeposition are scarcely found in the literature. Li *et al.* [29] reported that when the amount of carbonyl groups on carbon fibers was increased by thermal treatment, the amount of Cu nuclei on carbon during the Cu electrodeposition also increased. This could be also a way of increasing the dispersion of Cu nuclei on carbon as smaller nanoparticles.

In previous work by these authors [48], core-shell carbon-supported Pt(Cu) and Pt-Ru(Cu) nanoparticles were synthesized in three steps: 1) Cu electrodeposition on Vulcan carbon XC-72R; 2) Pt deposition on Cu by galvanic exchange; and 3) spontaneous deposition of Ru species on Pt. It was shown that this way allowed us to significantly reduce the Pt content of the catalyst together with increasing the CO tolerance. Thus, the CO stripping peak potentials were about 0.1 and 0.2 V more negative than those corresponding to the Pt/C and the Ru-decorated Pt/C catalysts, respectively. In addition, the efficiency of methanol oxidation per unit mass of Pt was much higher. In this paper, the effect of the electrochemical carbon oxidation on the synthesis of the core-shell Pt(Cu) and Pt-Ru(Cu) nanoparticles has been explored in order to try to effect a further improvement in the catalyst performance. Carbon Vulcan XC-72R was electrochemically oxidized under different conditions to increase the amount of oxygenated carbon groups and then the core-shell catalysts were deposited on it, using the best conditions reported in our previous work. The oxidized carbons and the catalysts thus prepared were characterized by means of structural and electrochemical techniques. The hydrogen adsorption/desorption behavior and the CO oxidation performance of these new catalysts were compared to those previously reported for the untreated carbon support.

2. Results and Discussion

2.1. XPS Analyses and Electrochemical Testing of Carbon Oxidation

Cyclic voltammograms of Vulcan carbon XC72R in 0.5 M H_2SO_4 were recorded between the initial potential of 0.0 V *vs.* RHE and different anodic limits up to 2.2 V to select the potentials to check its activation performance. Figure 1 shows that the anodic current in the anodic sweep significantly increased from about 0.9 V and passed through a maximum at about 2.0 V (curve *a*). According to this behavior, potentials of 1.6, 1.8, 2.0, and 2.2 V were tentatively selected as characteristic potentials for the anodic treatment of carbon.

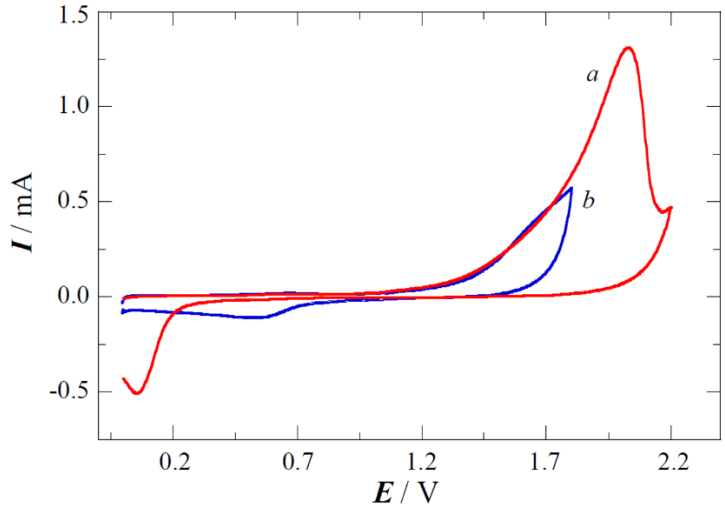

Figure 1. Cyclic voltammograms corresponding to the oxidation of Vulcan Carbon XC72R at 10 mV s^{-1} in 0.5 M H_2SO_4. The initial potential was 0.0 V and the reversal potential was (***a***) 2.2 V and (***b***) 1.8 V.

Figure 1 also highlights that the cathodic profile depended on the reversal potential. For the anodic limit of 1.8 V (curve *b*), the current in the cathodic sweep started to grow from about 0.7 V, passing through a rather flat cathodic peak at about 0.4–0.6 V. When the reversal potential was 2.2 V, the cathodic peak was close to 0.1 V. These curves then showed that the carbon oxidation was a function of the anodic limit. Note that in both cases, the charge of the anodic sweep largely exceeded the cathodic charge invested in the reduction of the species generated, thereby indicating the irreversibility of the oxidation process. This irreversible nature was further confirmed when performing consecutive cyclic voltammograms, in which a significant current decrease was apparent cycle by cycle (not shown here). It has been reported in the literature that the cathodic peak currents in the range 0.4–0.6 V are due to the reduction of the quinone phenolic groups of carbon to hydroquinone [18,19,35,36,38,42–45]. When the anodic and the cathodic limits were limited to the range 0.4–0.7 V, the transformation between quinone and hydroquinone groups appeared to be reversible. However, when the anodic potential exceeded 0.7 V in the positive direction, an increasing degree of carbon oxidation took place, as expected, along with the production of aldehyde and carboxylic groups and, finally, CO_2 evolution. For an anodic limit of 2.2 V, practically no cathodic current appeared between 0.4 and 0.6 V, suggesting the irreversible oxidation of most of the phenolic quinone groups to higher oxidation states.

XPS analyses of the oxidized carbons were performed in order to more precisely define the nature of the processes taking place at different potentials. The general spectra of the different carbons, including the non-oxidized one, showed only the presence of carbon and oxygen, although very residual amounts of S and Cl were also identified for the non-oxidized carbon. The main difference between the latter and the oxidized carbons was the oxygen content. The corresponding atomic ratio O:C was 0.62, 22.8, 22.0, and 22.3 atom % for the non-oxidized carbon and for carbons oxidized for 300s at 1.8, 2.0, and 2.2 V, respectively. The C1s and the O1s binding energy region of the XPS spectra are depicted in Figure 2a,b, respectively.

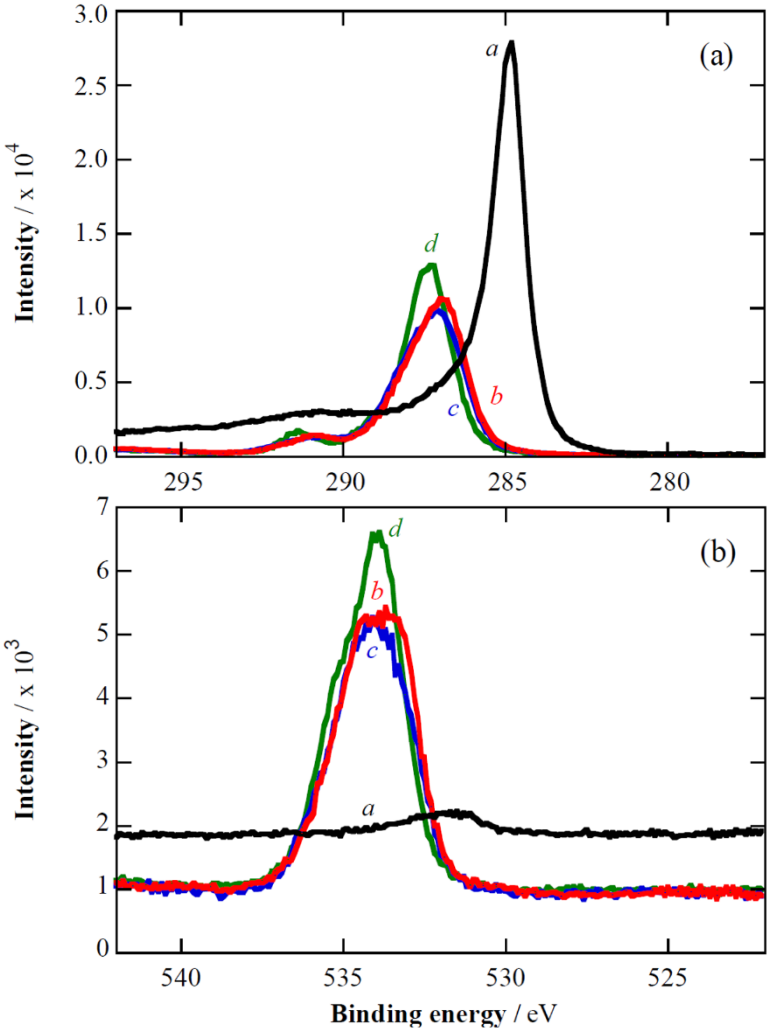

Figure 2. XPS spectra in the (**a**) C1s and (**b**) O1s binding energy region for the non-oxidized carbon (*a*) and the carbons oxidized at 1.8 V (*b*), 2.0 V (*c*), and 2.2 V(*d*).

In the C1s binding energy region (Figure 2a), it is clear that the surface carbon appears mainly in the form of the C–C state (284.5 eV) [19,49,50] for the non-oxidized carbon (curve *a*), whereas for the oxidized carbons, the binding energies are consistent with the states C–O (286.0 eV), C=O (287.8 eV) and O–C=O (290.2 eV) [19,51,52]. All the surface carbon appears to be oxidized. The chemical states of O1s (Figure 2b) are consistent with C–OH (531.8 eV) for the non-oxidized carbon (curve *a*), whereas for the oxidized carbons, O1s is mainly in the states O–C–O (532.2 eV) and O–C=O (534.3 eV) [19,51,52]. Note that when the oxidation potential of the carbon is increased, there is a shift

toward higher binding energies, thus indicating that the final oxidation form as CO_2 is approached. Moreover, the band located in the range 290–292 eV is due to the π electrons of the aromatic rings, in agreement with the presence of quinonic and hydroquinonic structures [53].

Further confirmation of the above behavior was found from the chronoamperograms depicted in Figure 3a, where the steady current depended on the applied potential. For potentials up to 2.0 V, small steady currents were obtained (curves *a*–*c*), whereas for 2.2 V (curve *d*) the current was one order of magnitude greater. Figure 3b shows that the profile of the cathodic sweep after the constant oxidation potential for 300 s of Figure 3a was consistent with the cyclic voltammograms shown in Figure 1. Reduction of phenolic quinone groups was apparent at about 0.4–0.6 V when the applied potentials were 1.6 and 1.8 V. The absence of significant reduction peaks at 0.4–0.6 V together with the formation of new cathodic peaks at more negative potentials, curves *c* and *d* in Figure 3b, clearly indicate that higher oxidation states of carbon were produced when the carbon was previously oxidized at 2.0 and 2.2 V, in agreement with the XPS analyses. The reduction of higher oxidized states was also apparent at constant potential oxidation of 1.8 V, as indicated by the big reduction peak at about 0.2 V. Oxidation at 2.0 and 2.2 V clearly led to deeper carbon oxidation including the formation of CO_2, species that were not reduced during the cathodic sweep.

The different carbon activation treatments described in the experimental part are associated to Figures 1 and 3: Figure 3a corresponds to treatment (i); Figure 3a followed by 3b, to treatment (iii); and 10 consecutive cycles following the first one shown in Figure 1, to treatment (ii). Figure 4 depicts the cyclic voltammograms of the oxidized carbons in the potential region from 0.0 to 1.0 V, which is the region of interest when analyzing the performance of the catalysts prepared in this paper. The main feature shown in the curves of Figure 4 is the Q/HQ couple (oxidation and reduction in the ranges 0.5–0.7 and 0.4–0.6 V, respectively), which is not apparent in curve *a* for the non-oxidized carbon. The symmetry of the peaks and charge of the anodic and the cathodic profiles corroborates the reversibility of the couple from 0.0 to 1.0 V. The cycles were also repetitive, thus proving the stability of the resulting carbon in these conditions. As can be seen in Figure 4a, the anodic and cathodic charges of the cyclic voltammograms increased when carbon was previously oxidized following the treatment (i) (curves *b*–*d*). The corresponding currents grew when changing the treatment potential from 1.6 to 2.0 V (curves *b* and *c*, respectively). However, the current decreased when the applied potential was 2.2 V (curve *d*), probably due to the more intense carbon degradation favoring its loss at this potential. The anodic and cathodic currents after treatment (iii) were similar to those obtained after treatment (i). Qualitatively similar features were found for treatment (ii) (Figure 4b), where the currents increased with the anodic limit of the potential cycling (curves *b* and *c*). In this case, the currents for an anodic limit of 2.2 V were higher than those obtained for treatment (i) at the same potential (curve *d* in Figure 4a). This can be explained assuming that the application of 2.2 V for 300 s produced higher carbon oxidation than potentiodynamic cycling 10 times up to the same potential. The formation of a higher amount of superior oxidation states of carbon, even with CO_2 evolution, involving a carbon loss and a decrease in the content of quinone groups, would explain the smaller currents of curve *d* in Figure 4a with respect to curve *c* in Figure 4b. Note that the highest peak currents reached in the cyclic voltammograms after all the carbon oxidation treatments were about 65 μA.

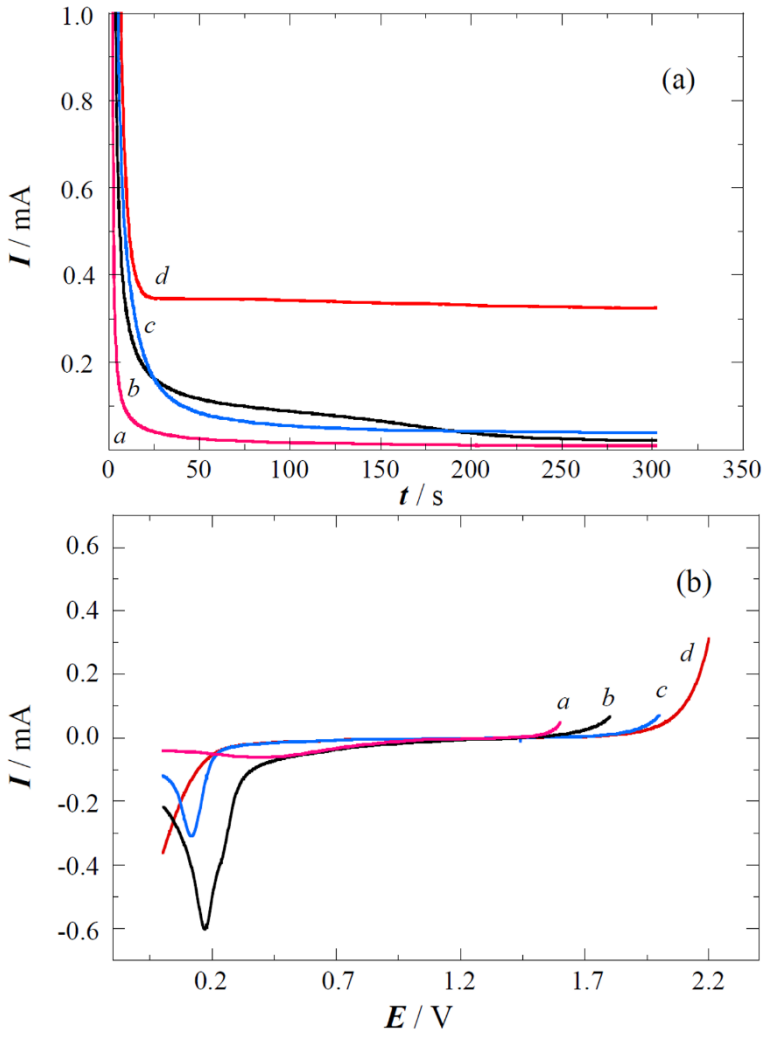

Figure 3. (**a**) Chronoamperograms obtained for the oxidation of Vulcan Carbon XC72R in 0.5 M H_2SO_4 at potentials: (*a*) 1.6 V, (*b*) 1.8 V, (*c*) 2.0 V, and (*d*) 2.2 V; (**b**) Cathodic sweep voltammograms at 10 mV s^{-1} up to 0.0 V after the potentiostatic oxidation of carbon for 300 s shown in (a), the initial potential being: (*a*) 1.6 V, (*b*) 1.8 V, (*c*) 2.0 V, and (*d*) 2.2 V.

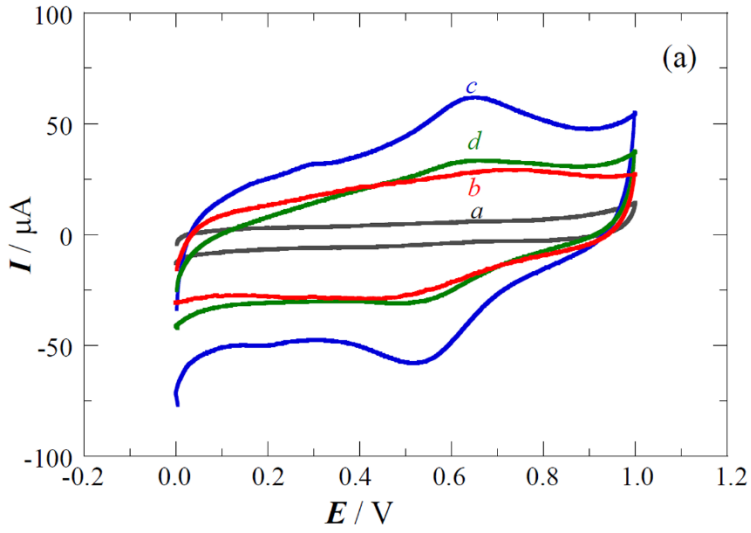

Figure 4. *Cont.*

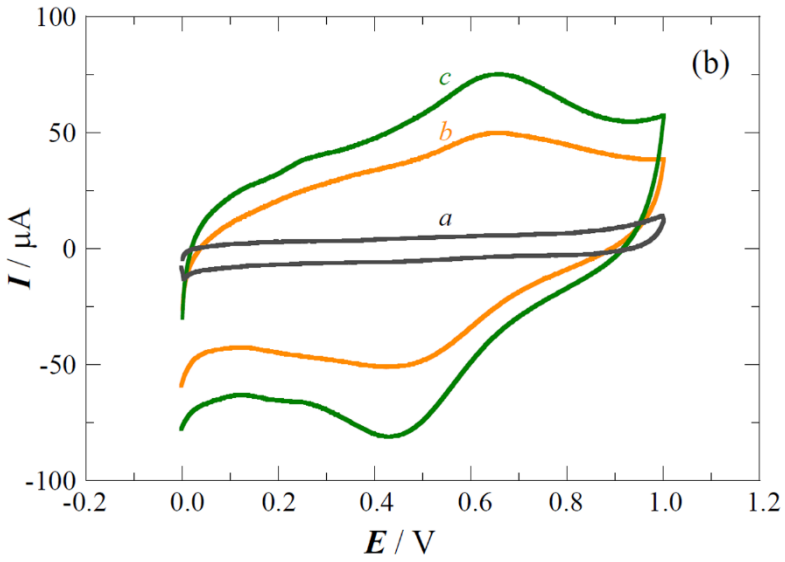

Figure 4. Cyclic voltammograms of carbon XC72R in deaerated 0.5 M H_2SO_4 at 20 mV s^{-1} after the different oxidation treatments. (**a**) Treatment (i), 300 s at (*b*) 1.6 V, (*c*) 2.0 V, and (*d*) 2.2 V; (**b**) Treatment (ii), anodic limit of (*b*) 1.8 V and (*c*) 2.2 V. Curves *a* in both graphics are the cyclic voltammograms of XC72R without previous oxidation treatment.

2.2. Copper Electrodeposition on the Oxidized Carbon

After the different activation treatments of carbon, 40 mC of Cu were electrodeposited at –0.1 V, as explained in the experimental part, and reoxidized in the same electrolyte to determine the copper electrodeposition efficiency. The corresponding voltammograms thus obtained are presented in Figure 5, where it can be observed that the copper oxidation profiles depended on the previous carbon oxidation. The Cu oxidation voltammograms on treated carbons presented anodic peaks that are wider and have much smaller peak currents than the reference curve *a* for the non-oxidized carbon. Treatments (i) (curves *b* and *c*) and (iii) (curves *d* and *e*) led to similar Cu oxidation profiles, with a peak and a shoulder at about 0.50 and 0.65 V, respectively. For treatment (ii) (curves *f* and *g*), the voltammograms were even more depressed, with still significant anodic currents at 1.0 V. This behavior was more pronounced at higher anodic limits and the treatment (ii) was not then found to be suitable for further examination and testing.

Peaks with an anodic maximum and a shoulder were also found during the reoxidation of electrodeposited copper on non-treated carbon for scan rates over 20 mV s^{-1} [48]. They were assigned to the formation of Cu^{2+} complexes and to the oxidation of the Cu(I) species generated by a disproportionation reaction, respectively. This double peak structure is not so apparent in curve *a* of Figure 5 because of the smaller scan rate. However, both, peak and shoulder, which were the main peak at about 0.50 V and the noticeable peak at about 0.65 V, were observed in the voltammograms of copper oxidation on the previously oxidized carbons, which could then be tentatively related to the same species as the untreated one. The shift of the anodic peaks and shoulder in the anodic direction could be explained considering that the oxidized carbons have a more open structure, with the possibility to nucleate copper in the inner part of the carbon spherules with a higher bonding energy because of the new oxygen-containing functional groups. The oxidation of the Cu nuclei could then be more difficult

and demand the application of higher potentials. In fact, it is reasonable to assume that the higher currents found after carbon oxidation in the cyclic voltammograms of Figure 4 were in part faradaic (Q/HQ couple) and also capacitive (expansion of the carbon structure). This expansion of the carbon structure would justify the formation of less accessible Cu nuclei, which, together with a higher bonding energy, would demand higher oxidation potentials for Cu oxidation.

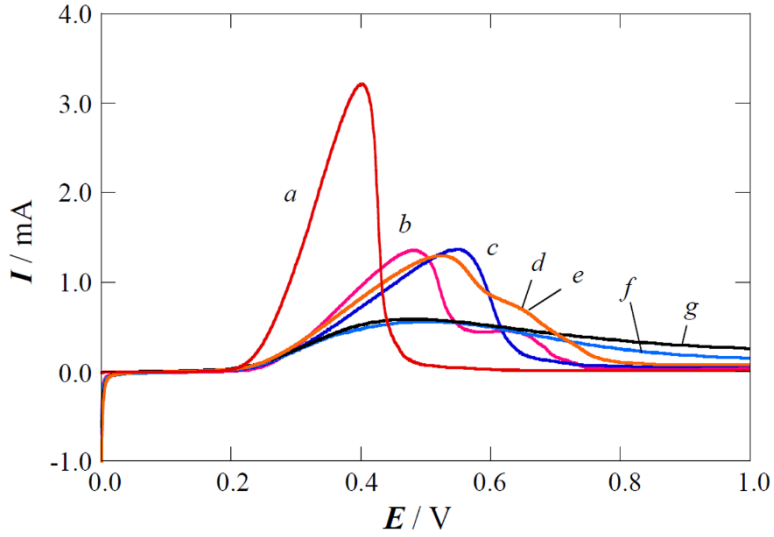

Figure 5. Cu oxidation voltammograms at 10 mV s^{-1} after 40 mC electrodeposition at −0.1 V in the same electrolyte (1.0 mM $CuSO_4$ + 0.1 M Na_2SO_4 + 0.01 M H_2SO_4). Experiments performed with carbon submitted to treatment (i): (*b*) 1.8 V, 300 s and (*c*) 2.2 V, 300 s; treatment (iii): (*d*) 1.8 V, 300 s and (*e*) 2.2 V, 300 s; and treatment (ii): cycling up to (*f*) 1.8 V and (*g*) cycling up to 2.2 V. Curve *a* is the reference one, obtained without previous oxidation of the carbon.

The anodic charges of the different voltammograms were measured to determine the current efficiencies of copper electrodeposition. In contrast to the untreated carbon, in which they were over 99% [48], the current efficiencies for oxidized carbons were somewhat smaller. For treatment (i) at potentials in the range 1.6–2.0 V for 300 s, the efficiency was about 86%. This can be explained by a small contribution of the reduction of oxidized carbon groups previously generated during the anodic treatment of carbon, which would take place in parallel with the Cu electrodeposition. This is in agreement with other electrodeposition experiments using carbon oxidized for shorter times. Thus, in the carbon oxidation at 1.6 and 1.8 V for 100s, the electrodeposition efficiency was about 95%.

The TEM images corresponding to the copper electrodeposition on the carbon oxidized following the treatment (i) at 1.6 V for 200 s and 2.2 V for 300 s, are depicted in Figure 6, where it is highlighted that Cu nuclei were obtained in the nanoparticle size. Figure 6b corresponds to 1.6 V, showing a HRTEM image with the FFT analyses of the squared marked area in the same figure. From the FFT analyses, the interplanar space *d* obtained was 0.2065 nm, which can be assigned to the planes Cu(100) ($d = 0.2088$ nm) [54], with a relative error of 1.1%. The size distributions of the nanoparticles are also shown in the insets, with respective mean sizes of 6.6 ± 3.1 and 4.4 ± 1.3 nm for 1.6 and 2.2 V, respectively. These nanoparticle sizes were comparable but somewhat higher than the mean value of 3.9 nm obtained in our previous work under the same Cu electrodeposition conditions, except for the carbon oxidation treatment [48].

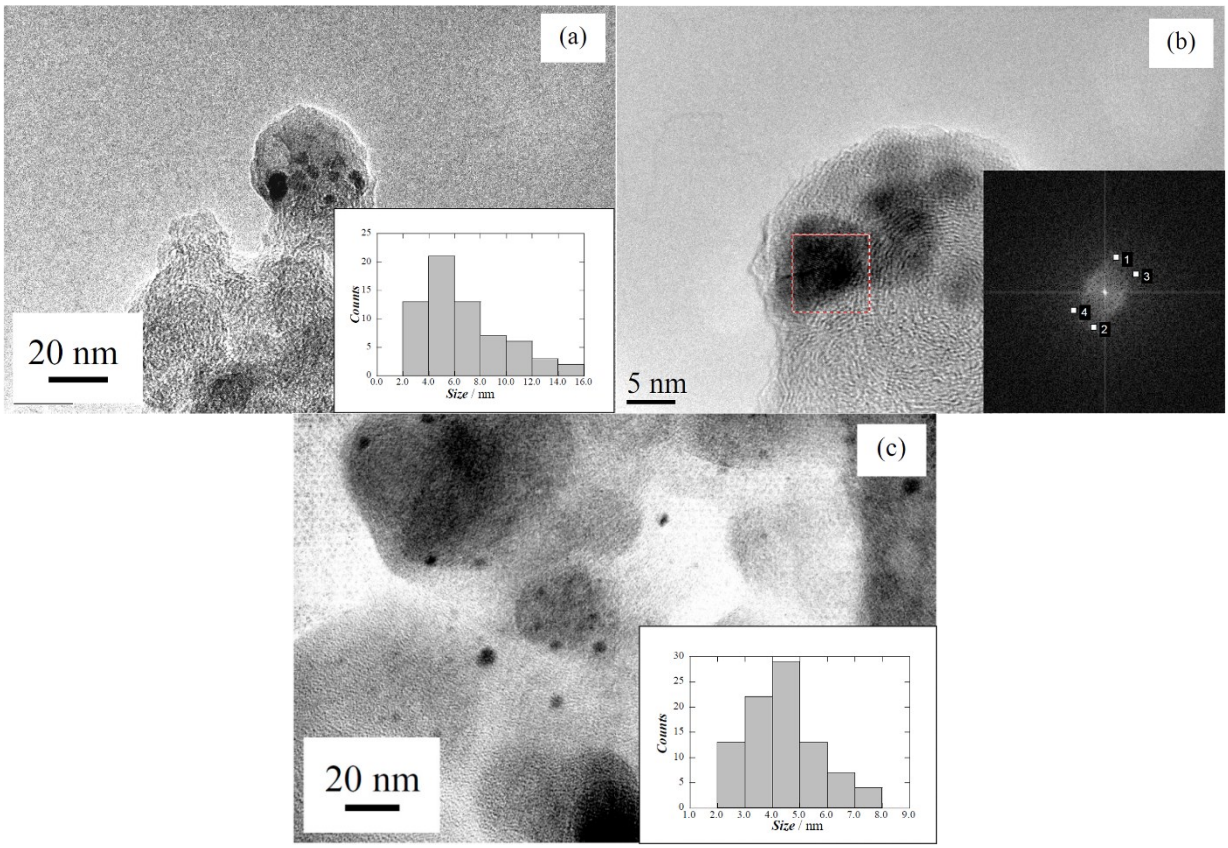

Figure 6. TEM micrographs of electrodeposited Cu on XC72R previously oxidized following treatment (i) at (**a**) and (**b**) 1.6 V, 200 s; (**c**) 2.2 V, 300 s. The size distributions are shown in the inset panels. Picture (**b**) is a HRTEM image from the sample shown in (**a**).

In order to examine how carbon oxidation can affect the size of the nanoparticles, one can suppose that the new oxygen-containing functional groups produced by carbon oxidation acted as additional nucleation centers for Cu electrodeposition. In this case, the electrodeposition of a given amount of Cu on the oxidized carbon would give a higher number of Cu nanoparticles, which should have a smaller size when compared to the non-oxidized one. As long as the nanoparticle sizes were not smaller for the oxidized carbons, one can infer that carbon oxidation did not lead to an increased number of nucleation centers for Cu electrodeposition. In the present case, it seems that the new oxygen-containing functional groups, behaving as nucleation centers, even yielded somewhat bigger nanoparticles. This interesting point undoubtedly merits more attention but is outside the scope of the present paper.

2.3. Performance of the Pt(Cu) and Pt-Ru(Cu) Catalysts

The prepared carbon-supported Pt(Cu) and Pt-Ru(Cu) catalysts were tested by cyclic voltammetry in 0.5 M H_2SO_4. Some examples are shown in Figure 7, where curves *a* and *c* correspond to Pt(Cu) with previous carbon oxidation according to treatment (i) (1.6 V for 200 s) and without oxidation treatment, respectively. Note that the surface Cu, if present, should be oxidized from a potential of about 0.2 V [48]. Since there is no evidence about it in the quasistationary curves shown in this figure, one can conclude that the cyclic voltammograms resulted only from the surface Pt, which is consistent with the expected core-shell structure.

It can also be observed that the currents were much higher with previous carbon oxidation. However, it is apparent that there is an important contribution of the capacitive charge effect due to the increase in area by the carbon oxidation together with the Q/HQ couple in the region of 0.4–0.7 V (see Figure 4). The respective mean charges of the hydrogen adsorption/desorption regions led to ECSA values of 1.58×10^3 and 0.66×10^3 m^2 mol_{Cu}^{-1} (see Table 1). The much higher ECSA value for previously oxidized carbon is indicative of a higher ability for the hydrogen adsorption/desorption process. This effect was general because in all cases, as shown in Table 1, carbon oxidation always gave higher ECSA values for hydrogen adsorption/desorption. In any case, the highest ones were obtained for treatment (i) at 1.6 V. Note that similar profiles can be observed in the cyclic voltammograms *a* and *c* of Figure 7 for the oxidized and the non-oxidized carbon, respectively, thus suggesting that carbon oxidation leads to a higher efficiency in the use of Pt and not to a different Pt structure on the surface of the nanoparticles. This is not surprising because carbon appears to be expanded with carbon oxidation and, therefore, protons could easily reach the Pt sites to be reduced.

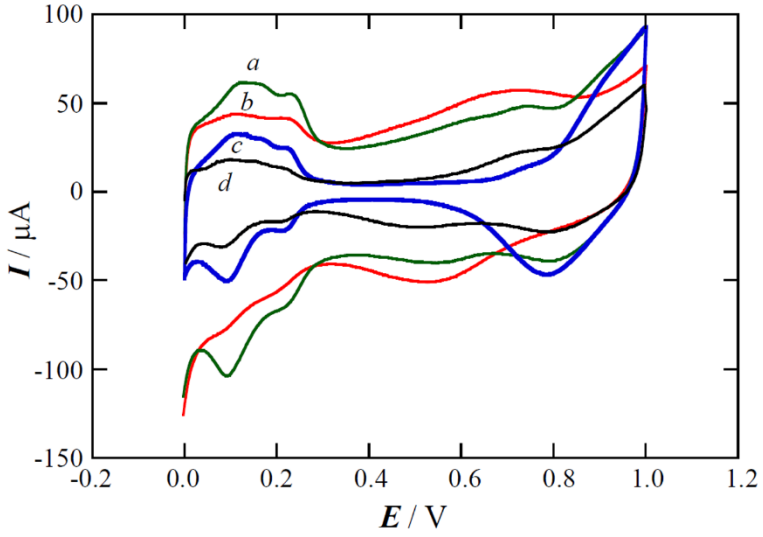

Figure 7. Cyclic voltammograms in 0.5 M H_2SO_4 at 20 mV s^{-1} for Pt(Cu)/C (curves *a* and *c*) and Pt-Ru(Cu)/C (curves *b* and *d*). Curves *a* and *b* correspond to the carbon submitted to treatment (i) at 1.6 V for 200 s, whereas curves *c* and *d* were obtained for carbon without previous oxidation.

The CO stripping curves corresponding to the same Pt(Cu) specimens as in Figure 6 are depicted in curves *a* and *c* of Figure 8, also for the carbon oxidized according to treatment (i) at 1.6 V for 200 s and for the non-oxidized carbon, respectively. Note that there was a capacitive shift of curve *a* toward higher currents, but the onset potential for CO oxidation was comparable to that obtained for the non-oxidized carbon. Table 1 highlights that the ECSA values for CO stripping were in general comparable to those obtained for the non-oxidized carbon. However, for carbon oxidation, they were also similar to those found for hydrogen adsorption/desorption, which is not the case for the non-oxidized carbon. The highest value was again obtained for 1.6 V (1.77×10^3 m^2 mol_{Cu}^{-1}), approximately equal to that measured for the non-oxidized carbon (1.79×10^3 m^2 mol_{Cu}^{-1}). Increasing the potential and time for carbon oxidation generally caused a decrease in the ECSA values. Moreover, no further improvement was found when changing treatment (i) by treatment (iii).

Table 1. Electrochemical active surface areas for hydrogen adsorption/desorption ($ECSA_{Hads/des}$) and for CO stripping ($ECSA_{CO}$), determined from the cyclic voltammograms in 0.5 M H_2SO_4 for the different catalysts and carbon oxidation treatments (i) and (iii). Results relative to the non-oxidized carbon have been taken from Ref. [48].

Carbon treatment	Catalyst	$ECSA_{Hads/des}$/ 10^3 m^2 mol_{Cu}^{-1}	$ECSA_{CO}$/ 10^3 m^2 mol_{Cu}^{-1}
no oxidation	Pt(Cu)	0.66	1.79
(i) 1.6 V, 100 s		1.56	1.55
(i) 1.6 V, 200 s		1.58	1.77
(iii) 1.6 V, 200 s		1.33	1.47
(i) 1.8 V, 300 s		1.27	1.50
(i) 2.0 V, 300 s		1.19	1.64
(iii) 2.0 V, 300 s		1.11	1.04
(i) 2.2 V, 300 s		1.05	1.16
(iii) 2.2 V, 300 s		1.05	1.18
no oxidation	Pt-Ru(Cu)	0.24	1.74
(i) 1.6 V, 200 s		0.62	1.73
(i) 2.2 V, 300 s		0.57	1.32

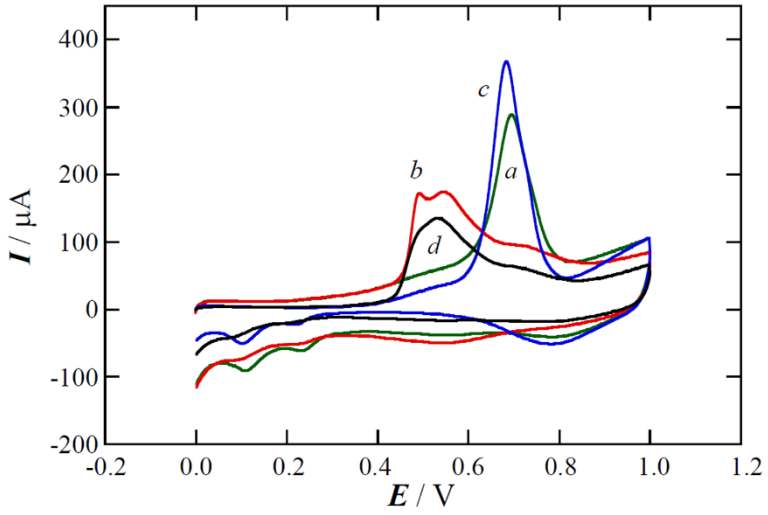

Figure 8. CO stripping voltammograms in 0.5 M H_2SO_4 at 20 mV s^{-1} for Pt(Cu)/C (curves *a* and *c*) and Pt-Ru(Cu)/C (curves *b* and *d*). Curves *a* and *b* correspond to the carbon submitted to treatment (i) at 1.6 V for 200 s, whereas curves *c* and *d* were recorded for carbon without previous oxidation.

The ECSA values for hydrogen adsorption/desorption and for CO oxidation were also measured after the spontaneous deposition of the Ru species. Cyclic voltammograms corresponding to hydrogen adsorption/desorption for the carbon oxidized according to treatment (i) at 1.6 V for 200 s and for the non-oxidized carbon, respectively, are shown in Figure 7. Curves *b* and *d* for Pt-Ru(Cu) presented a significant drop of the hydrogen adsorption/desorption currents with respect to curves *a* and *c* of Pt(Cu), because Ru species covering Pt sites were not suitable for hydrogen adsorption/desorption (see the ECSA values given in Table 1) [48,55]. The CO stripping curves for Pt-Ru(Cu) are depicted in Figure 8, where

curves *b* and *d* correspond to the carbon oxidized from the treatment (i) at 1.6 V for 200 s and to the non-oxidized carbon, respectively. The higher currents for the oxidized carbon can again be interpreted as due to the capacitive effect discussed above. However, no further improvement in the onset potential or in the ECSA value for CO oxidation (see Table 1) was found when compared to the non-oxidized carbon.

Micrographs of the Pt(Cu) and Pt-Ru(Cu) catalysts prepared on the carbon oxidized following treatment (i) at 1.6 V for 200 s are shown in Figure 9. The size distributions of the Pt(Cu) and the Pt-Ru(Cu) nanoparticles are given in the insets of Figure 9a,c, with mean particle sizes of 4.2 ± 1.3 and 3.3 ± 1.0 nm, respectively. Figure 9b depicts the FFT analyses of these Pt(Cu) nanoparticles, which gave interplanar spaces *d* of 0.2154 nm, which can be assigned to Pt(111) (*d* = 0.2265 nm) [54,55], with a relative error less than 5%. This interplanar space of Pt can be explained by the effect of the remaining Cu core, which has a smaller interplanar distance and can condition the structure of the Pt shell, in agreement with the expected core-shell structure.

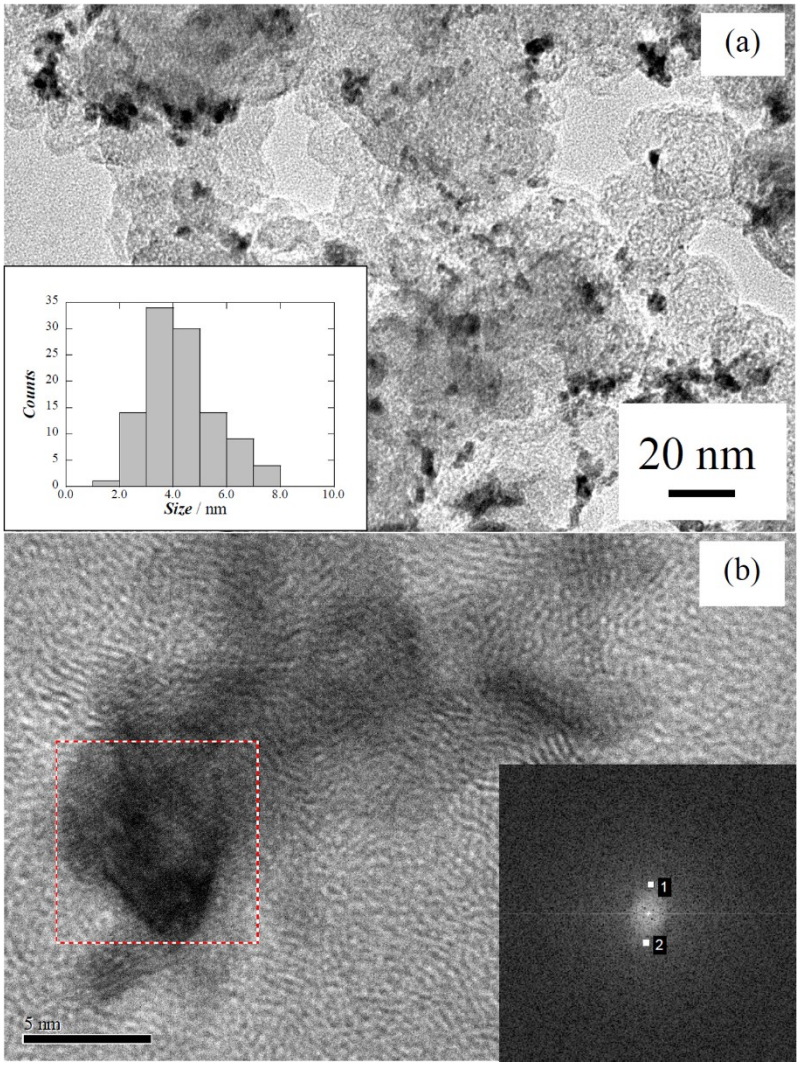

Figure 9. *Cont.*

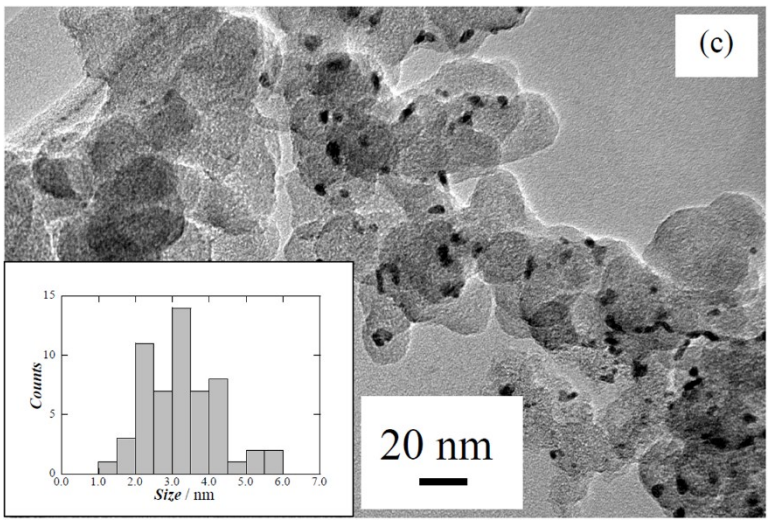

Figure 9. TEM micrographs of (**a**) and (**b**) Pt(Cu), and (**c**) Pt-Ru(Cu) electrocatalysts deposited on carbon oxidized following treatment (i) at 1.6 V, 200 s. The size distributions are shown in the inset panels. Picture (**b**) is a HRTEM image of the same sample shown in (a), which includes the corresponding FFT analysis of the marked zone.

Comparative images of the Pt(Cu) and the Pt-Ru(Cu) catalysts obtained on carbons oxidized following treatment (i) at 2.2 V for 300 s are presented in Figure 10. The corresponding nanoparticle size distributions are highlighted in the insets of Figure 10a,b, with values of 6.6 ± 1.2 and 4.8 ± 1.7 nm, respectively. These values were somewhat higher than those obtained for the same treatment at 1.6 V for 200 s, thus suggesting again that an increased carbon oxidation favored the nucleation of the metal particles around the oxidized points in the carbon and, therefore, the nanoparticle dispersion was somewhat smaller. The HRTEM image of Figure 10c allowed us to obtain the FFT analysis shown in the inset, with a mean interplanar space of d = 0.2208 nm, which can be assigned to Pt(111) (d = 0.2265 nm) [54,55] with a relative error of 2.5%.

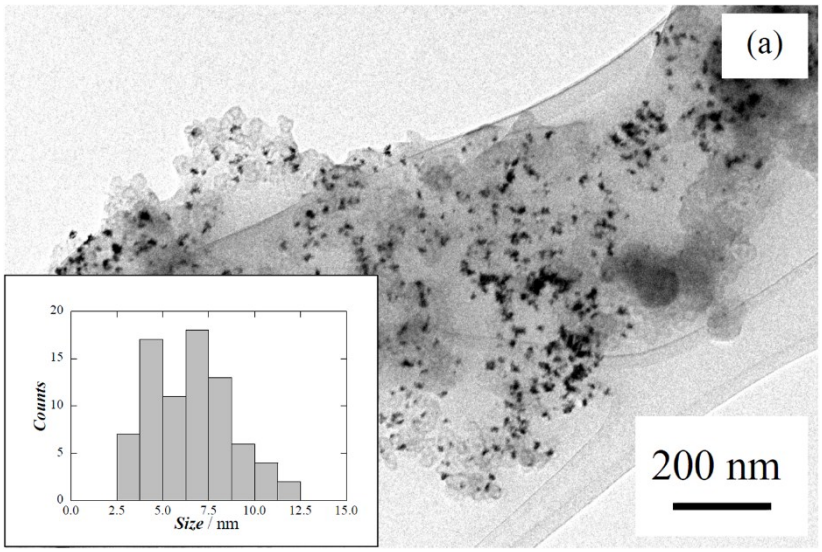

Figure 10. *Cont.*

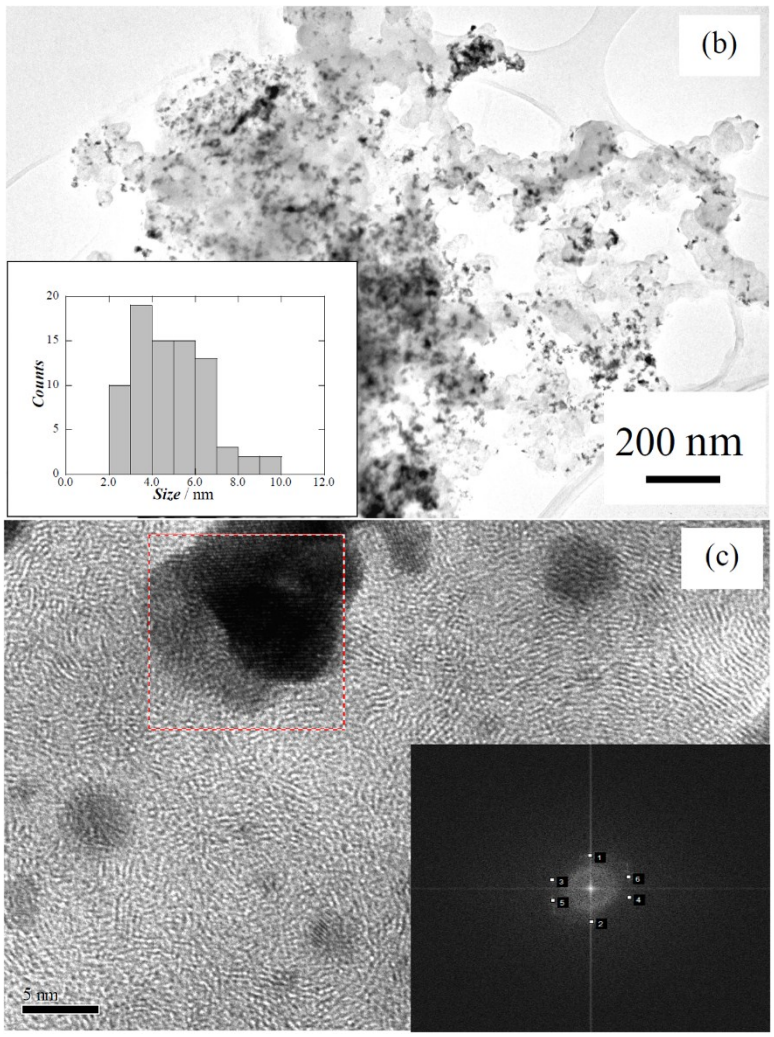

Figure 10. TEM micrographs of (**a**) Pt(Cu) and (**b**) Pt-Ru(Cu) electrocatalysts deposited on carbon oxidized following treatment (i) at 2.2 V, 300 s. The size distributions are shown in the inset panels. Picture (**c**) is a HRTEM image of the same sample shown in (**b**), which includes the corresponding FFT analysis of the marked zone.

The mean particle sizes and EDS analyses of the Pt-Ru(Cu) catalysts are summarized in Table 2. Apart from the nanoparticle size being somewhat higher when applying 2.2 V for 300s, in agreement with the discussion pointed out above, the EDS analyses showed the presence of the three elements, with a significant amount of Cu and a small quantity of Ru. The amount of Cu in all the specimens, together with the cyclic voltammograms shown in Figures 7 and 8, which do not give any evidence of Cu oxidation [48], were consistent with the core-shell structure. On the other hand, the poor quantity of Ru resulted from a slight surface deposition on Pt. This feature, together with the probable amorphous character of the deposited Ru species, could justify the fact that no Ru species were identified by the FFT analyses presented in Figure 10b [22,56].

Table 2. Mean particle sizes and EDS analyses of the Pt-Ru(Cu) specimens obtained on carbon oxidized according to treatment (i), compared to the non-oxidized carbon reported in Ref. [48].

Carbon treatment	Particle size/nm	Pt:Ru:Cu/at%
no oxidation	3.6	61.2:0.3:38.5
1.6 V, 200 s	3.3 ± 1.0	63.2:4.3:32.5
2.2 V, 300 s	4.8 ± 1.7	49.4:7.4:43.2

As can be seen in Table 2, the mean nanoparticle sizes and the EDS analyses were comparable to the results obtained for the non-oxidized carbon previously reported by us [48] and therefore, no further improvement with respect to them was obtained by means of the previous carbon oxidation treatment. One can then conclude that the oxidation treatments of carbon do not lead to smaller particle size, nor to a different structure or composition being able to further improve the CO tolerance and ECSA for CO oxidation with respect to the non-oxidized carbon. Note, however, that the CO tolerance continued to be as good as for the non-oxidized carbon, the onset potential for CO oxidation of Pt(Cu)/C and Pt-Ru(Cu)/C catalysts still being about 0.1 and 0.2 V more negative than those corresponding to Pt/C and Ru-decorated Pt/C ones, respectively [48]. Moreover, the improved results of the hydrogen adsorption/desorption ECSAs for the oxidized carbons when compared to the non-oxidized ones indicated a better electrolyte accessibility for the former, thus encouraging us to further test their catalyst performance in a real fuel cell.

3. Materials and Methods

3.1. Materials and Reagents

The test electrodes were prepared from E-Tek Vulcan XC72R carbon (mean particle size *ca*. 30 nm and specific surface area of about 250 $m^2\ g^{-1}$ [37]), which was deposited onto a Metrohm glassy carbon (GC) tip 3 mm in diameter. The GC was polished by means of Micropolish II deagglomerated α-alumina (0.3 μm) and γ-alumina (0.05 μm) on a Buehler PSA-backed White Felt polishing cloth. The solutions were prepared using Millipore Milli Q high-purity water (resistivity > 18 MΩ cm at 25 °C), analytical grade 96 wt.% H_2SO_4 from Acros Organics (Geel, Belgium), $HClO_4$, hydrated $RuCl_3$, and H_2PtCl_6 from Merck (Darmstadt, Germany), and $CuSO_4.5H_2O$, and Na_2SO_4 from Panreac Química S.A. (Barcelona, Spain). N_2 and CO gases were Abelló Linde 3.0 (purity ≥ 99.9%, Barcelona, Spain).

3.2. Working Electrodes and Electrochemical Testing

The electrochemical cells for the preparation of the working electrodes and testing were Metrohm 200 mL in capacity with a double-wall to control the temperature at 25.0 ± 0.1 °C by means of a Julabo MP-5 thermostat. The reference and auxiliary electrodes were a double junction Ag|AgCl|KCl(sat) (0.199 V *vs*. SHE at 25 °C) and a Pt rod, respectively. All the potentials given in this paper are referred to the Reversible Hydrogen Electrode (RHE). The working electrode was the carbon-supported catalyst, prepared using different electrolytes on the GC tip, which was coupled to an Ecochemie Autolab rotating disk electrode (RDE). The electrochemical experiments were conducted by means of an Ecochemie

Autolab PGSTAT100 potentiostat-galvanostat, commanded by a NOVA 1.5 software (Metrohm Autolab, Utrecht, The Netherlands). Before the electroless deposition of Pt and Ru species and the electrochemical tests using cyclic voltammetry (CV), a N_2 flow was bubbled through the electrolyte. This gas flow passed over the electrolyte during such deposition processes and measurements.

The working electrodes were prepared as previously described [48], except that activation was introduced here. In short, 4 mg of carbon were dispersed and sonicated in 4 mL of water for at least 45 min. Then, 20 μL of this suspension were deposited onto the polished GC tip (0.28 mg_C cm^{-2}) and dried under the heat of a lamp. Afterwards, the carbon was cleaned on the RDE in deaerated 0.5 M H_2SO_4 by CV scans between 0.0 and 1.0 V at 100, 50, and 20 mV s^{-1} for 10, 5, and 3 cycles, respectively (cleaning protocol). At this point and in the same electrolyte, three different activation procedures were applied: (i) potentiostatic oxidation of carbon for 100 s, 200 s, and 300 s up to 2.2 V; (ii) 10 consecutive cycles at 10 mV s^{-1} between 0.0 V and different anodic limits up to 2.2 V; and (iii) potentiostatic oxidation for 300 s at different potentials up to 2.2 V, followed by a potentiodynamic sweep at 10 mV s^{-1} to the cathodic limit of 0.0 V. After all of these activation treatments, the cleaning protocol was always applied.

After activation, the core-shell Pt(Cu)/C and Pt-Ru(Cu)/C catalysts were prepared according to the test results reported elsewhere [48], by the following consecutive steps: (a) potentiostatic deposition of Cu nuclei at −0.1 V and 100 rpm in 1 mM $CuSO_4$ + 0.1 M Na_2SO_4 + 0.01 M H_2SO_4 for 40 mC, determining the deposition efficiency of this Cu/C electrode through the Cu oxidation charge in the same solution after sweeping the potential from 0.0 to 1.0 V at 10 mV s^{-1}; (b) Pt deposition on the Cu nuclei by galvanic exchange in 1 mM H_2PtCl_6 + 0.1 M $HClO_4$ for 30 min at 100 rpm (Pt(Cu)/C electrode); and (c) spontaneous deposition of Ru species on the Pt(Cu)/C electrode in 8.0 mM $RuCl_3$ + 0.1 M $HClO_4$ (aged for at least one week) for 30 min without the electrolyte stirring (Pt-Ru(Cu)/C electrode). After the Cu deposition, the Cu/C electrode was carefully cleaned in water and, after steps (ii) and (iii), the Pt(Cu)/C and Pt-Ru(Cu)/C electrodes were also submitted to the cleaning protocol described above. It has to be noted that the cyclic voltammograms obtained from this protocol were always practically stationary after the second sweep, thus confirming the stability and cleanness of the electrodes.

The CO stripping curves for testing the CO oxidation activity and tolerance were performed in 0.5 M H_2SO_4, where CO gas was bubbled through the solution for 15 min, setting the electrode potential at 0.1 V. After removing the dissolved CO by N_2 bubbling through the solution for 30 min, CO was oxidized by sweeping the potential from 0.0 to 1.0 V at 20 mV s^{-1} without stirring. The electrochemically active area (ECSA) was estimated, taking into account that the oxidation of a CO monolayer on polycrystalline Pt needs 420 μC cm^{-2} [16,57]. After CO stripping, the activity of the Pt(Cu)/C and the Pt-Ru(Cu)/C catalysts was recovered, as shown by consecutive cyclic voltammograms, which retraced those obtained before the CO adsorption.

3.3. Microscopic Examination

The transmission electron microscopy (TEM) and high-resolution TEM (HRTEM) analyses were performed by means of a Hitachi H-800 MT, furnished with an Energy Dispersive X-ray (EDX) detector, and of a 200 kV JEOL JEM 2100 F, respectively. These analyses allowed for electron diffraction analyses and determining the size distribution, nanoparticle dispersion, and crystallographic phases. Prior to the observation, the catalyst on the GC tip was dispersed in 3 mL of *n*-hexane for 10 min by

ultrasonication. Then, a drop of the suspension was placed on a Holley-carbon nickel grid with further evaporation of the solvent under the heat of a 40 W lamp for 5 min. The images were recorded in a Gatan MultiScan 794 charge-coupled device (CCD) camera and the Fast Fourier Transform (FFT) analyses of selected areas were obtained by means of the Gatan Digital Micrograph 3.7.0 software. The MinCryst database was used to assign the crystallographic data corresponding to the electron diffraction and FFT. Different images from different zones allowed us to count more than 100 nanoparticles to determine their size distribution.

3.4. XPS Analyses

X-ray Photoelectron Spectroscopy analyses were performed using a Physical Electronics PHI 5500 Multitechnique System spectrometer with a monochromatic X-ray source (Al Kα line of 1486.6 eV, powered at 350 W). This X-ray source was placed perpendicular to the axis of the analyzer. The energy was calibrated using the 3d5/2 line of Ag with a full width at half maximum (FWHM) of 0.8 eV. The oxidized carbons, prepared as indicated above on the GC electrode, were carefully moved by scratching to the support, after careful cleaning in water and drying. The section for the surface analyses was a circular area of 0.8 mm in diameter. A survey spectrum (187.85 eV of Pass Energy and 0.8 eV/step) was first obtained and, afterwards, the high-resolution spectra (23.5 eV of Pass Energy and 0.1 eV/step) were recorded. A low energy electron gun less than 10 eV was used in order to discharge the surface when necessary. All the measurements were made in an ultra-high vacuum chamber pressure in the range 5.0×10^{-9}–2.0×10^{-8} torr. The resulting XPS spectra were analyzed using Ulvac-phi MultiPak V8.2B software.

4. Conclusions

This paper has explored the possibility of increasing the performance of electrodeposited Pt(Cu)/C and Pt-Ru(Cu)/C core-shell catalysts by previously oxidizing the carbon support. Different XC72R oxidation treatments were applied: (i) potentiostatic oxidation for 100–300 s up to 2.2 V; (ii) cycling 10 times at 10 mV s^{-1} between 0.0 and different anodic limits up to 2.2 V; and (iii) treatment (i) followed by a potentiodynamic sweep at 10 mV s^{-1} up to 0.0 V. The oxidation treatment led to a capacitive current increase in the potential range of interest between 0.0 and 1.0 V, together with the formation of Q/HQ couples. The XPS analyses of the oxidized carbons indicated an increase in the oxidation states of carbon with the anodic potential, tending to CO_2 formation. Cu electrodeposition as well as galvanic exchange with Pt and spontaneous deposition of Ru species was performed in the best conditions reported before for the non-oxidized carbon. The Cu reoxidation after its electrodeposition indicated that Cu nuclei presented a deeper penetration into a more open carbon structure, probably with a higher bonding energy when compared to the non-oxidized carbon. Treatment (ii) was not found to be suitable because Cu oxidation took place even after 1.0 V.

The Pt(Cu)/C and Pt-Ru(Cu)/C catalysts prepared following treatment (i) at 1.6 V for 200 s led to the best results of ECSA for the hydrogen adsorption/desorption and CO oxidation reactions. The EDX analyses of the latter gave 63.2, 32.5, and 4.3 atom % for Pt, Cu, and Ru, respectively. The HRTEM and FFT analyses of these catalysts showed smaller interplanar spaces for Pt due to the effect of the Cu core. The onset potential and the ECSA values for CO oxidation as well as the mean size of the catalyst

particles were comparably good to those obtained when using the non-oxidized carbon, and then behaved in a similar manner in front of the CO oxidation. However, the ECSA values for the hydrogen adsorption/desorption were much higher when carbon was previously oxidized. This was assigned not to a structural difference between the catalysts obtained with and without carbon oxidation, but to a better accessibility of the Pt sites. According to this, carbon oxidation appears to be useful to ensure a better catalyst performance.

Acknowledgments

The authors thank the financial support received from the *Generalitat de Catalunya* under the project 2014SGR83 as a consolidated research group and also that received from SENACYT (Republic of Panama) by Griselda Caballero-Manrique through the Scholarship Program for Professional Excellence. The authors also thank the CCiT-UB (Scientific and Technological Centers of the Universitat de Barcelona) for the electron microscope and the XPS analyses facilities.

Author Contributions

G.C.-M. and P.-L.C conceived and designed the experiments; G.C.-M. performed the experiments; G.C.-M, E.B., J.A.G., and P.-L.C. analyzed the data; F.C. and R.M.R. contributed reagents/materials/analysis tools; and G.C.-M., P.-L.C, and E.B. wrote the paper.

Conflicts of Interest

The authors declare no conflict of interest. The founding sponsors had no role in the design of the study; in the collection, analyses, or interpretation of data; in the writing of the manuscript; or in the decision to publish the results.

References

1. Antolini, E. Carbon supports for low-temperature fuel cell catalysts. *Appl. Catal. B* **2009**, *88*, 1–24.
2. Álvarez, G.; Alcaide, F.; Cabot, P.L.; Lázaro, M.J.; Pastor, E.; Sollá-Gullón, J. Electrochemical Performance of low temperature PEMFC with Surface Tailored Carbon Nanofibers as Catalyst Support. *Int. J. Hydrogen Energy* **2012**, *37*, 393–404.
3. Antolini, E. Platinum-based ternary catalysts for low temperature fuel cells. Part II. Electrochemical properties. *Appl. Catal. B* **2007**, *74*, 337–350.
4. Wang, Y.; Chen, K.; Mishler, J.; Cho, S.; Cordobes Adroher, X. A review of polymer electrolyte membrane fuel cells: Technology, applications, and needs on fundamental research. *Appl. Energy* **2011**, *88*, 981–1007.
5. Guo, J.W.; Zhao, T.S.; Prabhuram, J.; Chen, R.; Wong, C.W. Preparation and characterization of Pt-Ru/C nanocatalyst for direct methanol fuell cells. *Electrochim. Acta* **2005**, *51*, 754–763.
6. Salgado, J.R.C.; Alcaide, F.; Álvarez, G.; Calvillo, L.; Lázaro, M.J.; Pastor, E. Pt–Ru electrocatalysts supported on ordered mesoporous carbon for direct methanol fuel cell. *J. Power Sources* **2010**, *195*, 4022–4029.

7. Zainoodin, A.M.; Kamarudin, S.K.; Daud, W.R.W. Review: Electrode in direct methanol fuel cells. *Int. J. Hydrogen Energy* **2010**, *35*, 4606–4621.
8. Alcaide, F.; Álvarez, G.; Cabot, P.L.; Grande, H.J.; Miguel, O.; Querejeta, A. Testing of carbon supported Pd-Pt electrocatalysts for methanol electrooxidation in direct methanol fuel cells. *Int. J. Hydrogen Energy* **2011**, *36*, 4432–4439.
9. Yasuka, Y.; Fujiwara, T.; Murakami, Y.; Saaki, K.; Oguri, M.; Asaki, T.; Sugimoto, W. Effect of structure of carbon-supported PtRu electrocatalysts on the electrochemical oxidation of methanol. *J. Electrochem. Soc.* **2000**, *147*, 4421–4427.
10. Steigertwalt, E.; Deluga, G.; Cliffel, D.; Lukehart, C. A Pt-Ru/Graphitic carbon nanofiber nanocomposite exhibiting high relative performance as a direct-methanol fuel cell anode catalyst. *J. Phys. Chem.* **2001**, *105*, 8097–8101.
11. Dickinson, A.J.; Carrette, L.P.L.; Collins, J.A.; Friedrich, K.A.; Stimming, U. Preparation of Pt-Ru/C catalyst from carbonyl complexes for fuel cell applications. *Electrochim. Acta* **2002**, *47*, 3733–3739.
12. Friedrich, K.A.; Geiyzers, L.P.; Dickinson, A.J.; Stimming, U. Fundamental aspects in electrocatalysis: from the reactivity of single-crystals to fuel cell electrocatalysts. *J. Electroanal. Chem.* **2002**, *524–525*, 261–272.
13. Baena-Moncada, A.M.; Coneo-Rodríguez, R.; Calderón, J.C.; Flórez-Montaño, J.; Barbero, C.A.; Planes, G.A.; Rodríguez, J.L.; Pastor, E. Macroporous carbon as support for PtRu catalysts. *Int. J. Hydrogen Energy* **2014**, *39*, 3964–3969.
14. Velázquez-Palenzuela, A.; Centellas, F.; Garrido, J.A.; Arias, C.; Rodríguez, R.M.; Brillas, E.; Cabot, P.L. Kinetic analysis of carbon monoxide and methanol oxidation on high performance carbon- supported Pt-Ru electrocatalyst for direct methanol fuel cells. *J. Power Sources* **2011**, *196*, 3503–3512.
15. Boxall, D.L.; Deluga, G.A.; Kenik, E.A.; King, W.D.; Lukehart, C.M. Rapid synthesis of a Pt1Ru1/C nanocomposite using microwave irradiation: A DMFC anode catalyst of high relative performance. *Chem. Mater.* **2001**, *13*, 891–900.
16. Esparbé, I.; Brillas, E.; Centellas, F.; Garrido, J.A.; Rodríguez, R.M.; Arias, C.; Cabot, P.L. Structure and electrocatalytic activity of carbon-supported Pt nanoparticles for polymer electrolyte fuel cells. *J. Power Sources* **2009**, *190*, 201–209.
17. Min, M.; Cho, J.; Cho, K.; Kim, H. Particle size and alloying effects of Pt-based alloy catalysts for fuel cell applications. *Electrochim. Acta* **2010**, *45*, 4211–4217.
18. Tokarz, W.; Lota, G.; Frackowiak, E.; Czerwinski, A.; Piela, P. Fuel cell testing of Pt–Ru catalysts supported on differently prepared and pretreated carbon nanotubes. *Electrochim. Acta* **2013**, *98*, 94–103.
19. Álvarez, G.; Alcaide, F.; Miguel, O.; Cabot, P.L.; Martinez-Huerta, M.V.; Fierro, J.L.G. Electrochemical stability of carbon nanofibers in proton exchange membrane fuel cells. *Electrochim. Acta* **2011**, *56*, 9370–9377.
20. Hsieh, C.T.; Lin, J.Y.; Wei, J.L. Deposition and electrochemical activity of Pt-based bimetallic nanocatalysts on carbon nanotube electrodes. *Int. J. Hydrogen Energy* **2009**, *34*, 685–693.

21. Hwang, J.Y.; Chatterjee, A.; Shen, C.H.; Wang, J.H.; Sun, C.L.; Chya, O.; Chen, C.W.; Chen, K.H.; Chen, L.C. Mesoporous active carbon dispersed with ultra-fine platinum nanoparticles and their electrochemical properties. *Diam. Relat. Mater.* **2009**, *18*, 303–306.
22. Velázquez-Palenzuela, A.; Centellas, F.; Garrido, J.A.; Arias, C., Rodríguez, R.M.; Brillas, E.; Cabot, P.L. Structural characterization of Ru-modified carbon-supported Pt nanoparticles using spontaneous deposition with CO oxidation activity. *J. Phys. Chem. C* **2012**, *116*, 18469–18478.
23. Tegou, A.; Papadimitriou, S.; Pavlidou, E.; Kokkinidis, G.; Sotiropoulos, S. Oxygen reduction at platinum- and gold-coated copper deposits on glassy carbon substrates. *J. Electroanal. Chem.* **2007**, *608*, 67–77.
24. Papadimitriou, S.; Tegou, A.; Pavlidou, E.; Armyanov, S.; Valova, E.; Kokkinidis, G.; Sotiropoulos, S. Preparation and characterization of platinum- and gold-coated copper, iron, cobalt and nickel deposits on glassy carbon substrates. *Electrochim. Acta* **2008**, *53*, 6559–6567.
25. Rahsepar, M.; Pakshir, M.; Piao, Y.; Kim, H. Synthesis and electrocatalytic performance of high loading active PtRu multiwalled carbon nanotube catalyst for methanol oxidation. *Electrochim. Acta* **2012**, *71*, 246–251.
26. García, G.; Flórez-Montaño, J.; Hernández-Creus, A.; Pastor, E.; Planes, G.A. Methanol electrooxidation at mesoporous Pt and Pt-Ru electrodes: A comparative study with carbon supported materials. *J. Power Sources* **2011**, *196*, 2979–2986.
27. Ding, Y.; Liu, Y.; Rao, G.; Wang, G.; Zhong, Q.; Ren, B.; Tian, Z. Electrooxidation Mechanism of Methanol at Pt-Ru Catalyst Modified GC Electrode in Electrolytes with Different pH Using Electrochemical and SERS Techniques. *Chin. J. Chem.* **2007**, *25*, 1617–1621.
28. Yue, Z.R.; Jiang, W.; Wang, L.; Gardner, S.D.; Pittman, C.U., Jr. Surface characterization of electrochemically oxidized carbon fibers. *Carbon* **1999**, *37*, 1785–1796.
29. Li, W.; Liu, L.; Zhong, Ch.; Shen, B.; Hu, W. Effects of Carbon Fiber surface treatment on Cu electrodeposition: The electrochemical behavior and the morphology of Cu deposits. *J. Alloy Compd.* **2011**, *509*, 3532–3536.
30. Carmo, M.; dos Santos, A.R.; Rocha Poco, J.G.; Linardi, M. Physical and electrochemical evaluation of commercial carbon black as electrocatalysts supports for DMFC applications. *J. Power Sources* **2007**, *173*, 860–866.
31. Zhang, X.; Chan, K. Water in Oil microemulsion synthesis of platinum-ruthenium nanoparticles, their characterization and electrocatalytic properties. *Chem. Mater.* **2003**, *15*, 451–459.
32. Podlovchenko, B.I.; Krivchenk, V.A.; Maksimov, Y.M.; Gladysheva, T.D.; Yashina, L.V.; Evlashin, S.A.; Pilevsky, A. Specific features of the formation of Pt (Cu) catalysts by galvanic displacement with carbon nanowalls used as support. *Electrochim. Acta* **2012**, *76*, 137–144.
33. Podlovchenko, B.I.; Zhumaev, U.E.; Maksimov, Y.M. Galvanic displacement of copper adatoms on platinum in $PtCl_4^{2-}$ solutions. *J. Electroanal. Chem.* **2011**, *651*, 30–37.
34. Podlovchenko, B.I.; Gladysheva, T.D.; Filatov, A.; Yashina, L.V. The Use of Galvanic Displacement in Synthesizing Pt(Cu) Catalysts with the Core-Shell Structure. *Russ. J. Electrochem.* **2010**, *46*, 1189–1197.
35. Wang, J.; Yin, G.; Shao, Y.; Zhang, S.; Wang, Z.; Gao, Y. Effect of carbon black support corrosion on the durability of Pt/C catalyst. *J. Power Sources* **2007**, *171*, 331–339.

36. Weissmann, M.; Baranton, S.; Clacens, J.M. Coutanceau, C. Modification of hydrophobic /hydrophilic properties of Vulcan XC72 carbon powder by grafting of trifluoromethylphenyl and phenylsulfonic acid groups. *Carbon* **2010**, *48*, 2755–2764.
37. Cabot Corporation. Specialty Chemicals and Performance Materials. Available online: http://www.cabotcorp.com (accessed on 20 January 2014).
38. Kumar, S.; Soler Herrero, J.; Irusta, S.; Scott, K. The effect of pretreatment of Vulcan XC-72R carbon on morphology and electrochemical oxygen reduction kinetics of supported Pd nano-particle in acidic electrolyte. *J. Electroanal. Chem.* **2010**, *647*, 211–221.
39. Ghodbane, O.; Roué, L.; Bélanger, D. Copper electrodeposition on pyrolitic graphite electrodes: Effect of the copper salt on the electrodeposition process. *Electrochim. Acta* **2007**, *52*, 5843–5855.
40. Kumar, S.; Hidyatai, N.; Soler Herrero, J.; Irusta, S.; Scott, K. Efficient tuning of the Pt nano-particle mono-dispersion on Vulcan XC-72R by selective pre-treatment and electrochemical evaluation of hydrogen oxidation and oxygen reduction reactions. *Int. J. Hydrogen Energy* **2011**, *36*, 5453–5465.
41. Bae, G.; Youn, D.; Han, S.; Lee, J. The role of nitrogen in a carbon support on the increased activity and stability of a Pt catalyst in electrochemical hydrogen oxidation. *Carbon* **2013**, *51*, 274–281.
42. Yoon, Ch.; Long, D.; Jang, S.; Qiao, W.; Ling, L.; Miyawaki, J.; Rhee, Ch.; Mochida, I.; Yoon, S. Electrochemical surface oxidation of carbon nanofibers. *Carbon* **2011**, *49*, 96–105.
43. Gómez de la Fuente, J.L.; Martínez-Huerta, M.V.; Rojas, S.; Terreros, P.; Fierro; J.L.G.; Peña, M.A. Methanol electrooxidation on PtRu nanoparticles supported on functionalized carbon black. *Catal. Today* **2006**, *116*, 422–432.
44. Cao, J.; Song, L.; Tang, J.; Xu, J.; Wang, W.; Chen, Z. Enhanced activity of Pd nanoparticles supported on Vulcan XC72R carbon pretreated via a modified Hummers method for formic acid electrooxidation. *Appl. Surf. Sci.* **2013**, *274*, 138–143.
45. Yue, Z.R.; Jiang, W.; Wang, L.; Toghiani, H.; Gardner, S.D.; Pittman, C.U., Jr. Adsorption of precious metal ions onto electrochemically oxidized carbon fibers. *Carbon* **1999**, *37*, 1607–1618.
46. Carmo, M.; Linardi, M.; Rocha Poco, J.G. Characterization of nitric acid functionalized carbon black and its evaluation as electrocatalyst support for direct methanol fuel cell applications. *Appl. Catal. A* **2009**, *355*, 132–138.
47. Rueffer, M.; Bejan, D.; Bunce, N.J. Graphite: An active or an inactive anode? *Electrochim. Acta* **2011**, *56*, 2246–2253.
48. Caballero-Manrique, G.; Velázquez-Palenzuela, A.; Centellas, F.; Garrido, J.A.; Arias, C.; Rodríguez, R.M.; Brillas, E.; Cabot, P.L. Electrochemical synthesis and characterization of carbon-supported Pt and Pt-Ru nanoparticles with Cu cores for CO and methanol oxidation in polymer electrolyte fuel cells. *Int. J. Hydrogen Energy* **2014**, 39, 12859–12869.
49. Shao, Y.; Yin, G.; Zhang, J.; Gao, Y. Comparative investigation of the resistance to electrochemical oxidation of carbon black and carbon nanotubes in aqueous sulfuric acid solution. *Electrochim. Acta* **2006**, *51*, 5853–5857.
50. Yumitori, S. Correlation of C1s chemical state intensities with the O1s intensity in the XPS analysis of anodically oxidized glass-like carbon samples. *J. Mater. Sci.* **2000**, *35*, 139–146.

51. Stankovich, S.; Dikin, D.; Piner, R.; Kohlhaas, K.; Kleinhammes, A.; Jia, Y.; Wu, Y.; Nguyen, S.; Ruoff, R. Synthesis of graphene-based nanosheets via chemical reduction of exfoliated graphite oxide. *Carbon* **2007**, *45*, 1558–1565.
52. Yang, D.; Velamakannia, A.; Bozoklu, G.; Park, S.; Stoller, M.; Piner, R.; Stankovich, S.; Jung, I.; Fieldd, D.; Ventrice, C., Jr.; *et al*. Chemical analysis of graphene oxide films after heat and chemical treatments by X-ray photoelectron and Micro-Raman spectroscopy. *Carbon* **2009**, *47*, 145–152.
53. Terzyk, A. The influence of activated carbon surface chemical composition on the adsorption of acetaminophen (paracetamol) *in vitro*. Part II. TG, FTIR, and XPS analysis of carbons and the temperature dependence of adsorption kinetics at the neutral pH. *Colloids Surf. A* **2001**, *177*, 23–45.
54. WWW-MINCRYST. Crystallographic and Crystallochemical Database for Minerals and their Structural Analogues. Available online: http://database.iem.ac.ru/mincrysst (accessed on 30 June 2014).
55. Ruth, K.; Vogt, M.; Zuber, R. Development of CO-tolerant catalysts. In *Handbook of Fuel Cells—Fundamentals, Technology and Applications*; Vielstich, W., Gasteiger, H.A., Lamm, A., Eds.; John Wiley & Sons: New York, NY, USA, 2003; Volume 3, pp. 489–496.
56. Velázquez-Palenzuela, A.; Brillas, E.; Arias, C.; Centellas, F.; Garrido, J.A.; Rodríguez, R.M.; Cabot, P.L. Structural analysis of carbon-supported Ru-decorated Pt nanoparticles synthesized using forced deposition and catalytic performance toward CO, methanol, and ethanol electro-oxidation. *J. Catal.* **2013**, *298*, 112–121.
57. Chen, Z.; Xu, L.; Li, W.; Waje, M.; Yan, Y. Polianiline nanofibre supported platinum nanoelectrocatalysts for direct methanol fuel cells. *Nanotechnol.* **2006**, *17*, 5254–5259.